

Mixed Pixels Removal of a Laser Rangefinder for Mobile Robot 3-D Terrain Mapping

Cang Ye

Department of Applied Science, University of Arkansas at Little Rock, Little Rock, AR 72204, USA

Email: cxye@ualr.edu

Abstract—This paper presents an in-depth characterization of a direct time-of-flight Laser Rangefinder (LRF). It investigates several important characteristics of the LRF, such as the relationship between the intensity of the received signal and the range, the distribution and limited range effect of mixed pixels, and the evolution of the mixed pixel's range and intensity when a laser beam traverses the edge of an object. A method based on the discontinuity of the range and intensity is proposed to identify and remove the mixed pixels. An Extended Kalman Filter is designed to segment the range data and detect the range discontinuity. The proposed method is integrated with a terrain mapping and navigation system and tested in outdoor environments with a real mobile robot.

I. INTRODUCTION

Laser Rangefinders (LRFs) have been widely used in map-building for mobile robot navigation. In many of the research projects [1, 2], 2-D LRFs are used due to their affordability. Like other ranging device, A LRF exhibits errors in its range measurements. The range error of a LRF can be broadly classified into two categories: internal errors (drift with temperature, systematic and random errors) and external errors (caused by the interaction of the laser beam with the environment). The internal errors have received much attention and can be modeled [3, 4]. The external errors have been reported [5, 6] but have not been well characterized. One well-known and ubiquitous external error is a mixed pixel. When a laser beam hits the edge of an object, part of the beam is reflected by the front object and part by the background object. Both reflections are received by the LRF and result in a mixed measurement. The range measurement of a mixed pixel lies somewhere between the front and background objects. This means that a mixed pixel may generate substantially large range error. For 2-D occupancy map building [1], this range error should not create any problem as a mixed measurement caused a laser beam at the current robot's position may be removed by another laser beam at the next robot's position. However, for 3-D terrain mapping, each laser scan is new and the range data are accumulated. Therefore, range errors of mixed pixels are also accumulated in the terrain map. They may degrade the map

quality, cause misinterpretation of the 3-D scene, and deteriorate the performance of mobile robot navigation. This paper is intended to examine the mixed pixel phenomenon of a widely used 2-D LRF—Sick LMS 200—in robotics research community and to develop a practical method to remove the mixed pixels for terrain mapping and navigation.

The literature on characterization of the mixed pixel problem is scarce. In [7], Adams and Kerstens explicitly formulate the mixed pixel problem of a LRF (based on phase-shift measurement principle) in term of the areas of the laser spots on and the amplitudes of the received signals from the front and background objects. They propose a method to detect the discontinuity in amplitude and use the discontinuity information to remove the mixed pixels. The method requires the computation of the second derivative of the squared signal amplitude with respect to the area of the laser spot on the edge. Therefore, it requires several consecutive samples of the received signal when the laser beam traverses the edge. The method also assumes a constant surface reflectance factor during the traversing. Since the Sick LRF is a single pulse direct time-of-flight measuring system, we can only have one sample on the edge for each scan. This makes it impossible to apply their method to the Sick LRF. J. Tuley *et al.* [8] characterize the mixed pixel problem of a Sick LRF (LMS-291) in the environments with thin objects (smaller than the laser spot) and proposed an artifact removal method to filter out the mixed measurements. Their characterization study and the artifact removal method are merely based on the range information. Ye and Borenstein [9] investigate the mixed measurement phenomenon of the Sick LMS 200 and describe, in a qualitative manner, the way in which the range error evolves with the laser beam sweeps the edge of an object. Similar studies have been reported in [10, 11]. Up to date, all of the existing characterization studies have been merely focused on the range measurements of mixed pixels except for [7].

In this paper we characterize the mixed pixel phenomenon of the Sick LMS 200 by the measured range and signal intensity information. Since the knowledge of the internal physics and the hardware design such as how the system triggers a stop of the time counter of the LRF is not available, the characterization is performed in a qualitative way through experiments. This paper is organized as follows: In Section II the characteristics of the mixed measurements and the approach to removing mixed pixels are presented. In Section III an Extended Kalman Filter (EKF) is proposed to segment

This work was supported in part by NASA through Arkansas Space Grant Consortium under grant number UALR16800, NASA EPSCOR Planning and Preparatory Award, and a matching fund from the Office of Research and Sponsored Programs of the University of Arkansas at Little Rock (UALR).

C. Ye is with the Department of Applied Science, UALR, Little Rock, AR 72204, USA (phone: 501-683-7284; fax: 501-569-8020; e-mail: cxye@ualr.edu).

the range data for discontinuity detection. Then, in Sections IV the mixed pixel removal method is implemented in a complete mapping and navigation system and experimented with a real robot. Section V concludes the paper.

II. CHARACTERIZATION OF THE SICK LMS 200 LRF

In the author's previous characterization study [9] of the Sick LMS 200, the distribution of the range measurements on targets with various surface properties (surfaces with different colors and grey levels) and targets with different laser beam incidence angles were investigated. It was discovered that: (1) in both cases the distribution can be approximated by $N \sim (\mu, \sigma^2)$ with $\sigma_{max}=6$ mm and the deviation of μ from the true range value is less than 16 mm. (2) the incidence angle has a greater influence than the target surface property on μ . However, the difference is not substantial (the maximum deviation of μ from the true range for the former and the latter is 16 mm and 10 mm, respectively).

In the same work, the mixed pixel phenomenon is qualitatively studied through series of experiments. Specifically, a mixed pixel is observed when a laser beam hits the edge of an object (this situation is also called a corner shot). In this case, the reflection of the laser beam from the front and the background object are received by the LRF and produces a range measurement somewhere between the front object and the background. The range measurement moves closer to the background if the movement of the front object increases the area of the laser spot on the background. The mixed measurement can be anywhere between the front object and the background if the distance between the front object and the background ΔD is bigger than 20 cm but smaller than 1.6 meter [12]. Figure 1 depicts the number of mixed pixels (out of 4000 range measurements) versus ΔD

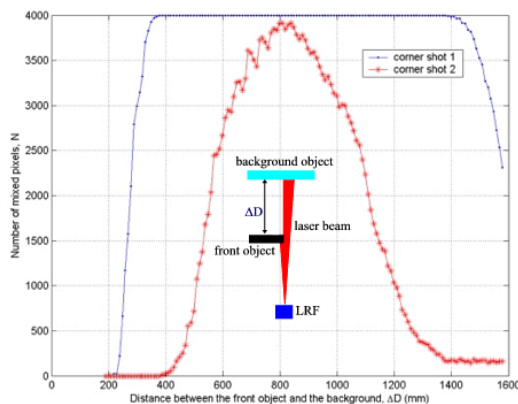


Fig. 1. Characteristics of mixed pixels. The front and background objects were placed in such a way that a mixed measurement was observed. 4000 range measurements were taken for each ΔD . A measurement is determined as a mixed measurement if the difference between the measured range and foreground/background is bigger than 60 mm. Large numbers of mixed pixels were generated when the distance ΔD between the edge of the foreground object and the background was close to the laser pulse's width ΔL . However, if $\Delta D > \Delta L$, then the number of mixed pixels drops significantly.

for two corner shots. It indicates that the mixed pixel problem has a limited range effect, i.e., the range error of a mixed measurement can not be over 1.6 meter. This is because the laser pulse's width of the Sick LRF is close to 1 meter. The LRF uses this pulse width as the signature of the returned signal to reject the ambient noise. This scheme induces a measurement window that allows the reflection from background (within the meter pulse width) to be received and thus results in a mixed measurement.

In summary, a mixed pixel has two features in its range values: (1) It has range discontinuity, i.e., the range value changes suddenly; and (2) the range differences between the mixed pixel and its neighboring data must be bigger than a threshold value (e.g., 6 cm) and smaller than 1.6 meter. Although the features are distinctive, they are not sufficient for removing mixed pixel. This is because in a clutter environment a discontinued range measurement may be generated by a true object lying between the front object and the background. To search for a practical approach to removing mixed pixels, the energy of the received signal (called direct reflectivity by the manufacturer) is investigated in this work. The Sick LRF can be configured to send out both the range and reflectivity values. Figure 2 depicts the

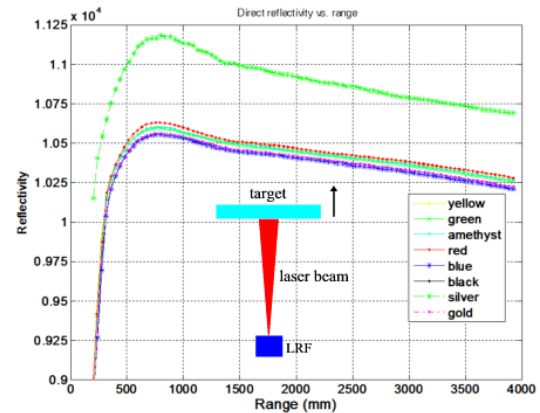


Fig. 2. Reflectivity versus range for targets with different colors. The target object was placed in such a way that the laser beam hits the target perpendicularly with a full laser spot. The target object was then moved away from the LRF at a 40 mm increment. The average reflectivity value and average true range over 1000 samples are plotted.

relationships between the reflectivity and the range for targets with various colors. It can be observed that the reflectivity decreases linearly with the increase of range (if range is larger than 800 mm). Due to coaxial optical alignment of the transmitter and the receiver, the reflectivity and range values do not exhibit the same relationship for a range that is smaller than 800 mm. Figure 2 also suggests that in most case color only has minor effect on the reflectivity. Targets with different grey levels ranging from white to black were also tested. The similar results were obtained. However, the spacing between plots with different grey levels is relatively bigger. This means that surface reflectance factor has a larger effect than surface color on the reflectivity values. This can be clearly seen in Fig. 2 where the plot of the silver target

(acts like a reflector) has a much larger reflectivity value for each target position.

Experiments were carried out to study the evolution of the range and reflectivity values when a laser beam “traverses” the edge of the front object (actually simulated by moving the front object in the lateral direction). Figure 3 depicts one of the typical results. In addition to the distinctive range discontinuity, we may observe that: (1) the reflectivity of a mixed pixel is larger than that of a normal measurement; and (2) for the mixed pixels with large range error (labeled in area *c* in Fig. 3a), the reflectivity values (Fig. 3b) are much larger than that of the front and background objects. These two features were clearly present in all experiments with targets having different surface properties and various laser beam incidence angles on the front and/or background objects, as long as the distance between the front objects and the LRF is bigger than 63 cm. Out of that value, the reflectivity of the front object drop down abruptly (see Fig. 2). In this case, the reflectivity of the background becomes dominant and the mixed measurement phenomenon is not noticeable (a range error less than 6 cm was observed in the experiments).

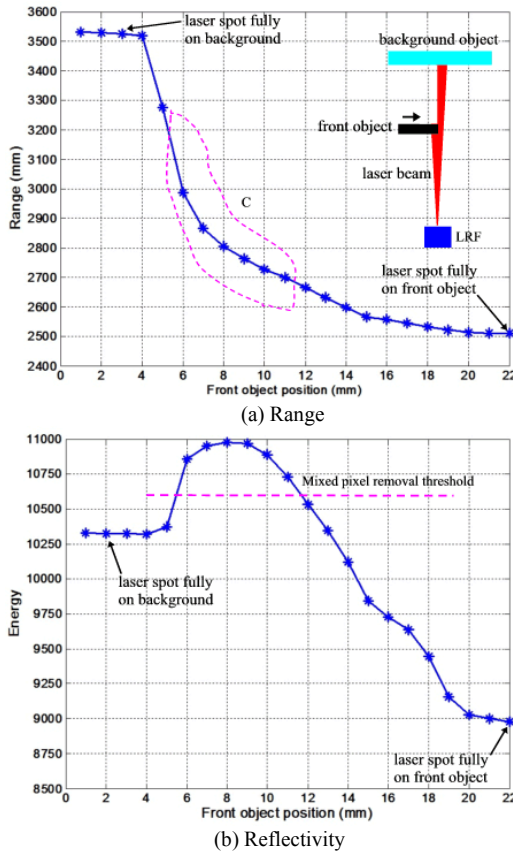


Fig. 3. Evolution of the range and reflectivity values of mixed pixels when the laser beam traverses the edge of the front object. The front object (black) and background object (white) were located about 2.5 meters and 3.5 meters away from the LRF. The front object was moved into the laser spot step by step (1 mm per step) from the right to produce mixed measurements.

The above-mentioned features of mixed pixels in the range and reflectivity values can be used as the signature of a mixed measurement and used to remove mixed pixels. Taking the

case in Fig.3 as an example, if the threshold value in Fig. 3b is used, then the measurements taken with the front object at position 6-11 will be identified as mixed pixels and removed, i. e., a measurement falling into area *c* in Fig. 3a will be removed as a mixed pixel. This treatment removes a mixed pixel with a range error bigger than 15 cm from the front object.

This paper assumes that the LRF interacts with objects with large surfaces (i.e., surfaces may accommodate several full laser spots). This assumption is valid in most indoor and outdoor urban environments. Under this condition, mixed pixels can be identified and removed by the following procedure: (1) Range data are first segmented into collinear segments and isolated points. (2) Each isolated point is compared with its left or right neighboring data that is on a line segment. If the difference in range is within 6~160 cm, then it is treated as a candidate mixed pixel. Otherwise, it is a normal data. (3) The reflectivity of each candidate mixed pixel is compared with that of its left and right neighboring data. If the difference in reflectivity is bigger than a threshold value (300 is used in this paper), then this candidate data is accepted as a mixed measurement and removed. Otherwise, it is kept as a normal data.

III. EKF FOR MIXED PIXELS DETECTION AND REMOVAL

In order to detect the discontinuity of range, the data segmentation method based on the Extended Kalman Filter (EKF) [16] is employed. The EKF method—based on a stochastic framework—effectively segments and identifies isolated pixels (potential mixed pixels or random noises) simultaneously. Considering the case that three consecutive laser data points, p_1 , p_2 , and p_3 forms a straight-line segment L_n on a flat ground surface, as shown in Fig. 4a, we have

$$l_{i+2} = \frac{l_i l_{i+1}}{2l_i \cos \delta - l_{i+1}}. \quad (1)$$

Let state variables $x_1(k)=l_{i+1}$ and $x_2(k)=l_i$, we obtain a two-sate nonlinear process model as follows:

$$x_1(k+1) = \frac{x_2(k)x_1(k)}{2x_2(k) \cos \delta - x_1(k)} + w_1(k) \quad (2)$$

$$x_2(k+1) = x_1(k) + w_2(k)$$

It can be written in the following vector form:

$$\mathbf{x}(k+1) = \mathbf{F}(\mathbf{x}(k)) + \mathbf{w}(k) \quad (3)$$

where $\mathbf{w}(k)$ is the process noise and is assumed to be $N \sim (0, \mathbf{Q})$. By expanding $\mathbf{F}(\cdot)$ as a Taylor series about the prediction $\hat{\mathbf{x}}(k|k)$ at time step k and neglecting higher order terms, we linearize the process model as

$$\Delta \mathbf{x}(k+1) \approx \mathbf{A} \Delta \mathbf{x}(k) \quad (4)$$

where $\Delta \mathbf{x}(k+1)=\mathbf{x}(k+1)-\mathbf{x}(k)$ and \mathbf{A} is the Jacobian matrix given by

$$\mathbf{A} = \begin{bmatrix} \frac{2\hat{x}_2^2(k) \cos \delta}{(2\hat{x}_2(k) \cos \delta - \hat{x}_1(k))^2} & \frac{-\hat{x}_1^2(k)}{(2\hat{x}_2(k) \cos \delta - \hat{x}_1(k))^2} \\ 1 & 0 \end{bmatrix} \quad (5)$$

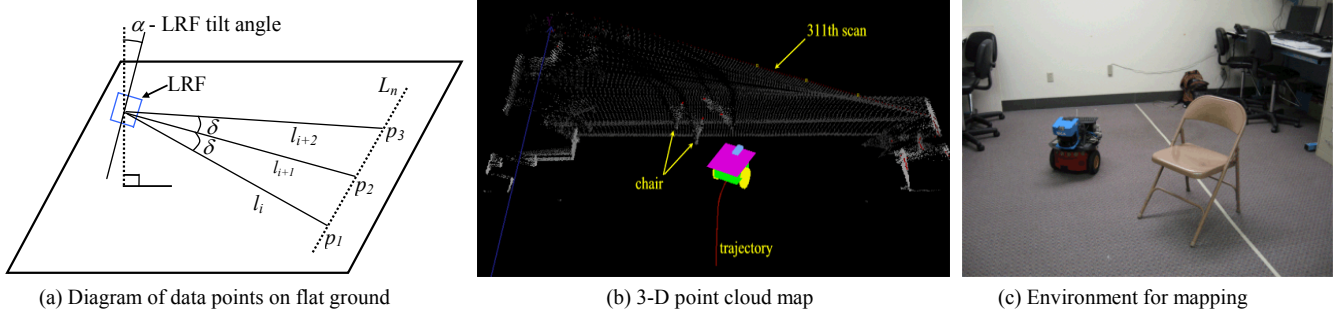


Fig. 4. Consecutive range data points form a straight-line on flat ground. (a) Three consecutive data points form a straight-line on a flat ground. (b) Data points collected from 311 scans represented in 3-D point cloud encoded by the reflectivity values, the brighter the point the bigger the reflectivity value. (c) The picture of the environment where the data in (b) were collected.

The linear range measurement equation is

$$z(k) = l_{i+1} = \begin{bmatrix} 1 & 0 \end{bmatrix} \begin{bmatrix} x_1(k) \\ x_2(k) \end{bmatrix} + v(k) = \mathbf{B}\mathbf{x}(k) + v(k) \quad (6)$$

where \mathbf{B} is the observation matrix, and $v(k)$ is the measurement noise which has a Gaussian distribution $N \sim (0, \sigma^2)$ [17] and is uncorrelated. The range data are then segmented into collinear point sets by the following EKF process:

- (1) The predicted measurement and the posteriori error covariance matrix are computed by

$$\hat{\mathbf{x}}(k+1|k) = \mathbf{F}(\hat{\mathbf{x}}(k|k)) \quad (7)$$

$$\mathbf{P}(k+1|k) = \mathbf{A}\mathbf{P}(k|k)\mathbf{A}^T + \mathbf{Q}$$

- (2) The innovation of the EKF is $y_k = \mathbf{B}\hat{\mathbf{x}}(k+1|k) - z(k+1)$.

Assuming that the errors of the predicted measurement $\mathbf{B}\hat{\mathbf{x}}(k+1|k)$ and the observation $z(k+1)$ are statistically independent, the innovation covariance is $S_k = \mathbf{B}_k \mathbf{P}_{k|k-1} \mathbf{B}_k^T + \sigma^2$. The square of the Mahalanobis distances ζ_k between the predicted measurement and observation is given by

$$\zeta_k = y_k^T S_k^{-1} y_k \quad (8)$$

We want to test the hypothesis H_0 : the predicted measurement and the observation represent the same point, i. e., $y_k=0$. We accept the hypothesis H_0 with confidence γ using a threshold value ε such that $P\{\zeta_k \leq \varepsilon | H_0\} = \gamma$. In other words, the new data point $z(k+1)$ is classified to be in the same process at a confidence of γ if $\zeta_k \leq \varepsilon$. As ζ_k has a χ^2 distribution, an appropriate threshold ε can be determined using a χ^2 table. For an instance, we declare $z(k+1)$ to be in the same process with a confidence of 0.95 if $\zeta_k \leq 3.84$ ($\varepsilon=3.84$). The filtering process continues until the event $\zeta_k > \varepsilon$ where the new data point is taken as an initial observation of a new process. In such an event, we take the previously filtered point as the end of the current collinear segment, and start a new process using the new measurement point as the starting point of the coming segment.

- (3) The Kaman Filter Gain is updated by

$$\mathbf{K}(k+1) = \mathbf{P}(k+1|k)\mathbf{B}^T S_k^{-1} \quad (9)$$

and the state vector and the posteriori state error covariance are updated by

$$\hat{\mathbf{x}}(k+1|k+1) = \hat{\mathbf{x}}(k+1|k) + \mathbf{K}(k+1)y_k \quad (10)$$

$$\mathbf{P}(k+1|k+1) = \mathbf{P}(k+1|k) - \mathbf{K}(k+1)\mathbf{B}\mathbf{P}(k+1|k).$$

$\mathbf{P}(k|k)$ and $\hat{\mathbf{x}}(k|k)$ are approximately chosen using the initial two range measurements at $k=1$ and $k=2$ of each process. The filter is initialized with $\hat{x}(2|2) = \begin{bmatrix} z(2) \\ z(1) \end{bmatrix}$ and

$$P(2|2) = \begin{bmatrix} \sigma^2 & 0 \\ 0 & \sigma^2 \end{bmatrix}.$$

The range data of each laser scan are segmented into straight-line segments if there are least three collinear data points in the same process and identified as isolated points otherwise. Figure 5 depicts the result of applying the segmentation method to the 311th scan of the laser data collected in the experiment as shown in Fig. 4. Each

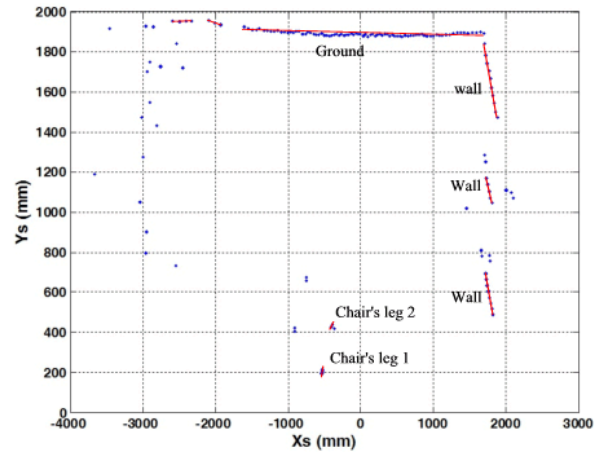


Fig. 5. Segmentation of the 311th scan of the data collected in the experiment as shown in figure 4.

straight-line segment indicates a group of collinear data points

IV. IMPLEMENTATION WITH A MOBILE ROBOT

The proposed mixed pixel removal method is integrated

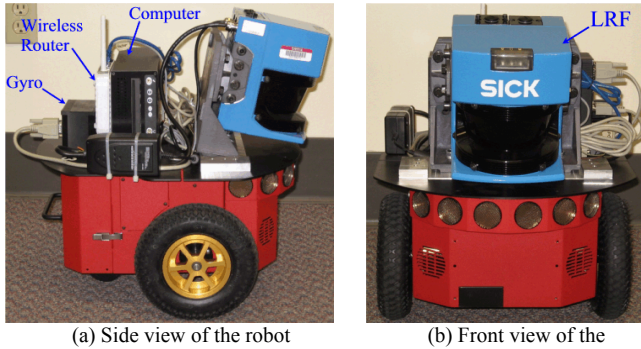


Fig. 6. The P3-DX robot equipped with sensors for mapping and navigation

with a complete terrain mapping and navigation system. A pioneer robot platform P3-DX (Fig. 6) is used for experiment. The robot has a differential drive mechanism and can turn with a zero turning radius. Since the experiments were conducted on uneven terrain, the robot's roll, pitch and yaw (Euler angles) must be sensed for position estimation and map-building. This is achieved by a 3-axis fiber optic gyro. The robot's roll, pitch and yaw angles, and its X , Y , and Z coordinates (called robot pose collectively) are then used to register the laser range data into a terrain map.

The on-board computer uses a 2.0 GHz Pentium 4 processor. It acquires the laser range data from the LRF (Sick LMS 200) at 500k baud and the robot Euler rate from the gyro at 38400 baud through a RS-422 card. It obtains the robot's wheel encoder data at 115200 baud through a regular RS-232 port. These data are then used for terrain mapping and navigation. The robot motion commands are determined by the navigation software based on the terrain map and used to control the robot. The onboard computer also transmits the robot pose and laser range data to an off-board laptop computer via the wireless router. The process of terrain mapping and navigation is thus visualized on the laptop computer in real-time.

Figure 7 shows the diagram of the entire navigation system that is used in the experiments. The proposed EKF-based mixed pixel removal algorithm is used as a data preprocessing unit at the front-end of the terrain mapping module. The navigation system consists of three main modules: Terrain Mapping, Terrain Traversability Analysis (TTA) and Path Planning. The vision sensor for terrain mapping is the Sick LRF that looks forward and downward at the terrain with an angle of -10° from the robot base plate. This configuration allows the robot to profile the terrain ahead by its motion.

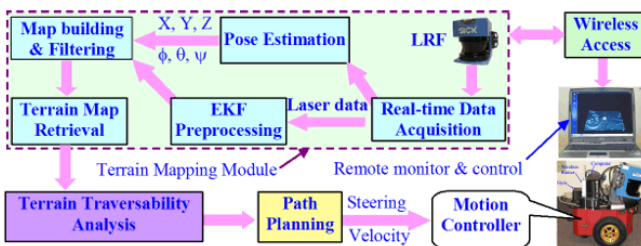


Fig. 7. Diagram of the navigation system: the module within the dashed lines is the Terrain Mapping module

Homogeneous coordinate transformation is used to register laser data into a 3-D terrain map.

The TTA module transforms the elevation map into a traversability map where each cell holds a value representing the degree of difficulty for the robot to move across that cell. This value is called Traversability Index (TI). The Path Planning module converts the traversability map into a number of Polar Traversability Indexes [2] (PTIs) each of which represents the level of difficulty for the robot to move along the corresponding direction. Based on the PTIs, the Path Planning module determines the steering and velocity commands of the robot and sends these motion commands to control the robot. The detail of the navigation method is referred to [2].

Experiments were carried out on outdoor terrain outside the Fribourgh Hall at the University of Arkansas at Little Rock. As shown in Fig. 8, the terrain is uneven and contains curbs and a ramp. A number of cardboard boxes were used to construct obstacle courses. A navigation task is specified to the robot by giving the robot its target location. The system is then initialized using the robot's current position as its start point (the robot X , Y , Z coordinates are reset to zero).

The Operating System used for the navigation system is RTLinux. The LRF's angular resolution is set to 1° . Each scan of the LRF takes 13.33 ms and contains 151 range and reflectivity data pairs, each of which covers a 151° field of view. The Real-time Data Acquisition (RDA) section in the terrain mapping module (Fig. 7) resides in the real-time Linux kernel as a real-time thread. The RDA thread buffers the LRF data, the gyroscopic data, and the wheel encoder data in a shared memory. Once it obtains 7 scans of laser data and the associated gyroscopic and encoder data, the Map-building and Filtering section fetches this data set; and registered the range data into a terrain map. The TTA module then obtains the local terrain map and transforms it into a traversability map. Then the path planning module converts the traversability map into a PTI histogram, determines the motion commands, and sends the commands to the robot. The above process repeats every 93.3 ms (7×13.33 ms) until the robot reaches the target.

Figure 8 shows one of the autonomous runs from S_3 to G_3 . S_3 has a higher elevation than G_3 . The area immediately before the ramp is in a valley that is lower than the neighboring area. The 3-D terrain map (rendered on the remote laptop computer) is depicted in Fig 8d in a form of color-coded point cloud where the dark blue points represent data with negative elevation (below S_3). The black spots are unperceived areas (no range data due to occlusion). The elevation values increase when the color changes from dark blue to purple and from purple to light yellow. (If displayed in black and white, a brighter point has a bigger elevation value.) Figure 8c displays the 2.5-D elevation map at the point where the robot was avoiding the first obstacle it encountered. Figure 8e shows the elevation map at the time when the robot was avoiding the curb and aligning itself with

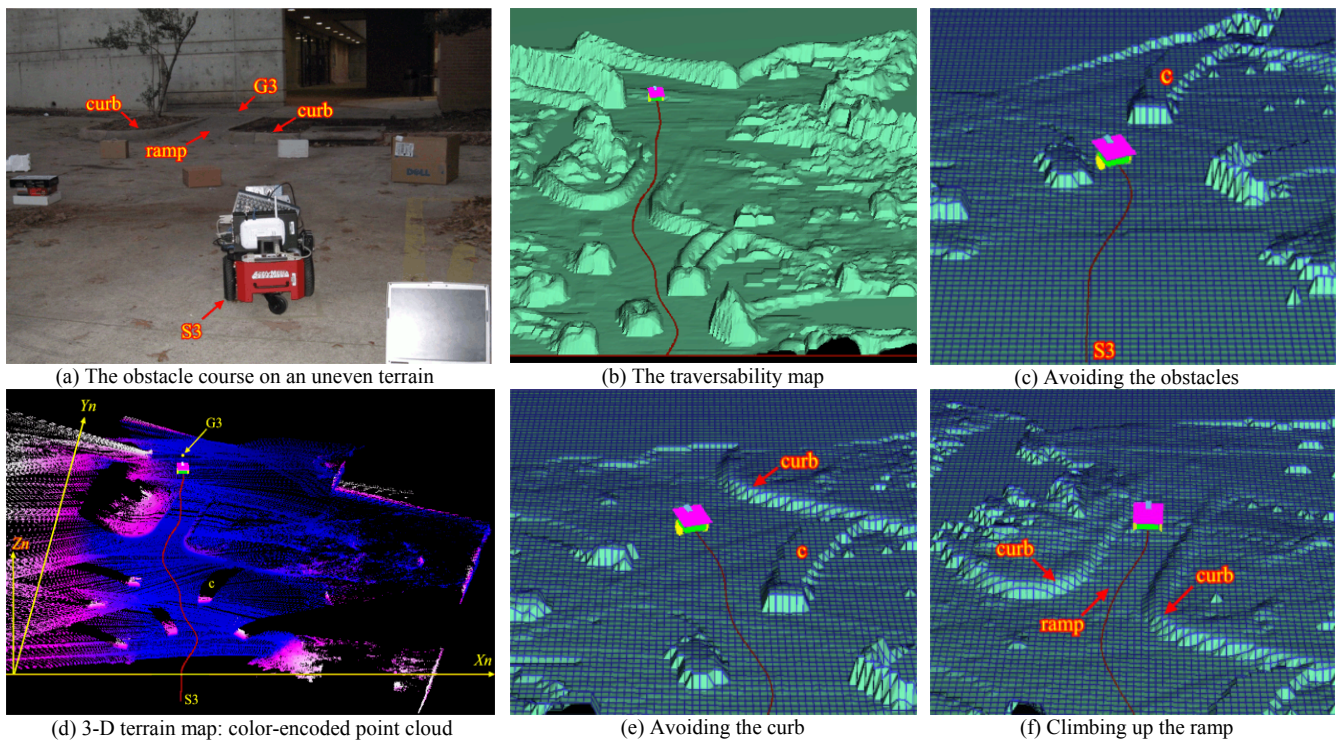


Fig. 8. Experiment on an outdoor terrain outside the Fribourgh Hall at UALR: The robot ran from S_3 to G_3 . The red curve represents the robot trajectory. The robot in (b) is just for illustration. It is actually a point in the traversability map.

the ramp. Figure 8f depicts the elevation map after the robot successfully traversed the ramp. In the elevation maps, the unperceived areas (e.g., c) of the lower terrain surface look like obstacles because their Z coordinate values (zero) are bigger than that of the surrounding terrain surfaces whose elevation values are negative. The path planning method in the navigation system actually uses the traversability map depicted in Fig. 8b to pilot the robot.

V. CONCLUSIONS

In conclusion, this paper presents an in-depth study on the characteristics of the Sick LMS 200. It investigates the mixed pixel phenomenon and proposes a method to identify and remove the mixed pixels based on the range and reflectivity information. An EKF segmentation algorithm is used to find the range discontinuity. The use of the mixed pixel removal method may enhance the terrain map. The proposed method has been integrated with a terrain mapping and navigation system and tested on a real robot in outdoor environments. The enhanced navigation system can be used to guide mobile robots/vehicles in urban environments for transport, surveillance, patrol, search and rescue, and military missions.

REFERENCES

[1] S. Thrun, D. Fox, W. Burgard, and F. Dellaert, "Robust Monte Carlo localization for mobile robots," *Artificial Intelligence*, 128 (1-2):99-141, 2000.
 [2] C. Ye, "Navigating a mobile robot by a traversability field histogram," *IEEE Transactions on Systems, Man, and Cybernetics-Part B: Cybernetics*, vol. 37, no. 2, pp. 361-372, 2007.

[3] D. Nitzan, et al, "The measurement and use of registered reflectance and range data in scene analysis," *Proceedings of the IEEE*, vol. 65, no. 2, 1977.
 [4] M.D. Adams and A.J. Kerstens, "The interpretation of phase and intensity data from AMCW light detection sensors for reliable ranging," *International Journal of Robotics Research*, Vol. 15, No.5, pp. 441-458, 1996.
 [5] M. Hebert and E. Krotkov, "3D measurements from imaging laser radars: how good are they?" *Image and Vision Computing*, vol. 10, no. 3, pp. 170-178, 1992.
 [6] A. Reina and J. Gozalez, "Characterization of a radial laser scanner for mobile robotic navigation", *Proc. IEEE/RSJ International Conference on Intelligent robots and systems*, 1997, pp. 579-585.
 [7] M. D. Adams, "Amplitude modulated optical range data analysis in mobile robotics," *Proc. IEEE International Conference on Robotics and Automation*, 1993, pp. 8-13.
 [8] J. Tuley, N. Vandapel and M. Hebert, "Analysis and removal of artifacts in 3-D LADAR data," *Proc. IEEE International Conference on Robotics and Automation*, 2005, pp. 2204-2210.
 [9] C. Ye and J. Borenstein, "Characterization of a 2-D laser scanner for mobile robot obstacle negotiation," *Proc. IEEE International Conference on Robotics and Automation*, 2002, pp. 2512-2518.
 [10] X. Luo and H. Zhang, "Characterization of Acuity Laser Range Finder," *Proc. International Conference on Control, Automation, Robotics and Vision*, 2004, pp. 2100-2104.
 [11] M. Alwan, M. B. Wagner, G. Wasson, and P. Sheth, "Characterization of Infrared Range-Finder PBS-03JN for 2-D Mapping," *Proc. IEEE International Conference on Robotics and Automation*, 2005, pp. 3936-3941.
 [12] C. Ye and J. Borenstein, "A novel filter for terrain mapping with laser rangefinders," *IEEE Transactions on Robotics*, vol. 20, no. 5, pp. 913-921, 2004.